

RESEARCH

Open Access



Regenerative potential of graphene oxide-chitosan nanocomposite combined with fetal bovine serum on healing of full-thickness skin wound in rats

Kamal H. Hussein^{1,2*}, Mahmoud Soliman³, Mahmoud S. Sabra⁴, Hani Nasser Abdelhamid⁵, Mahmoud Abd-Elkareem⁶ and Ahmed Abdelrahim Sadek¹

Abstract

Background Delayed wound closure and non-healing wounds represent a problematic condition with health burden and an economic challenge. Therefore, different strategies have been developed, including skin tissue engineering, which aims to stimulate and support the wound healing process. In this study, the potential of graphene oxide (GO) and chitosan (CTS) biomaterial composite, with and without fetal bovine serum (FBS), was investigated to induce a full-thickness skin wound repair in rats.

Methods The GO-CTS composite was characterized using X-ray diffraction, transmission electron microscopy, and Fourier transforms infrared. Cytocompatibility was evaluated via an MTT assay with human endothelial cells (ECs) and mouse embryonic fibroblasts (MEFs) in vitro. The in vivo wound regeneration potential was assessed by creating an 8 mm full-thickness circular skin defect on the dorsal surface of the rat. The defects were randomly divided into control, GO-CTS, FBS, and GO-CTS/FBS groups, and were monitored grossly and histologically at days 7 and 21 after wound induction.

Results The GO-CTS material demonstrated high cytocompatibility, with cell viability recorded at $99.2\% \pm 5.7\%$ for ECs and $110.5\% \pm 3.9\%$ for MEFs. The highest proliferation rates were observed in the FBS ($118.2\% \pm 2.1\%$) and GO-CTS/FBS ($121.4\% \pm 4.4\%$) groups. In vivo, wound closure rates on day 21 were $85.5\% \pm 0.56\%$ for GO-CTS, $87.5\% \pm 1.75\%$ for FBS, and $91.5\% \pm 1.03\%$ for GO-CTS/FBS, all significantly higher than the control group. Additionally, neovascularization, epithelialization, collagen deposition, and granulation tissue formation were more prominent in the treated groups, with skin appendages observed in the GO-CTS/FBS group.

Conclusion GO-CTS nanosheets with FBS represent a promising biomaterial for skin tissue engineering and can effectively initiate and support wound healing.

Keywords Graphene oxide, Chitosan, Wound healing, Skin tissue engineering, FBS, Cytocompatibility

*Correspondence:

Kamal H. Hussein
kamalhussein@aun.edu.eg

Full list of author information is available at the end of the article



© The Author(s) 2025. **Open Access** This article is licensed under a Creative Commons Attribution 4.0 International License, which permits use, sharing, adaptation, distribution and reproduction in any medium or format, as long as you give appropriate credit to the original author(s) and the source, provide a link to the Creative Commons licence, and indicate if changes were made. The images or other third party material in this article are included in the article's Creative Commons licence, unless indicated otherwise in a credit line to the material. If material is not included in the article's Creative Commons licence and your intended use is not permitted by statutory regulation or exceeds the permitted use, you will need to obtain permission directly from the copyright holder. To view a copy of this licence, visit <http://creativecommons.org/licenses/by/4.0/>.

Introduction

Injuries of the skin are a frequently reported affection of immense health care owing to the necessity of the skin in various physiological activities. The skin serves mainly as a physical barrier against external threats such as bacteria, fungi, viruses, radiation, and other harmful issues. Additionally, skin is crucial for vitamin D metabolism, regulation of body temperature, fluid balance, and immunological reactions [1, 2]. The occurrence of wounds resulting in damage to or removal of the skin, could predispose to scarring, wound infection, ulcer formation, and even gangrene [3, 4].

Skin has naturally evolved to heal wounds by restoring its protective barrier. Wound healing is a combinatorial process that needs the existence of suitable microenvironmental cues and a variety of interacting cells. The events of healing include orchestrated steps of inflammation, epithelialization, proliferation, angiogenesis, and remodeling. Throughout the healing process, fibroblasts, endothelial cells, platelets, and macrophages actively migrate, infiltrate, proliferate, and differentiate. This process leads to tissue growth and wound closure [4–7]. While natural skin regeneration often allows for normal healing, there are still several obstacles to rapid wound healing [1, 8]. These obstacles include infection, inadequate tissue oxygenation, limited vascularity, concurrent disease, and immunocompromised diseases [2, 9]. Hence, skin tissue engineering has emerged as a solution to hasten wound healing and overcome unfavorable healing outcomes. Skin tissue engineering implicates the integration of cells and growth factors into scaffolds to provide a favorable microenvironment for initiation of cell adhesion, migration, proliferation, and differentiation. The scaffold material should be biocompatible with suitable porosity [10, 11].

Two-dimensional nanomaterials such as graphene oxide (GO) are widely used in biomedicine, in particular tissue engineering [12, 13]. GO nanosheets are characterized by specific features such as high stability, good conductivity, high hydrophilicity, high drug loading capacity, and biocompatibility [14–17]. Thus, GO is incorporated alone or in combination with other materials in tissue engineering, including skin [2, 15, 18], bone [13], cartilage [19], skeletal muscles [20], and peripheral nerves [21]. It was also reported for photothermal treatment of wounds infected with pathogenic bacteria [22, 23].

Biopolymers have been considered a promising biomaterial for medical applications [6]. Chitosan (CTS) is a biopolymer derived from chitin and has desirable properties including excellent biodegradability, biocompatibility, antimicrobial activity, and minimal toxicity [24, 25]. CTS was fabricated into scaffolds that were applied in skin [26, 27], bone [28], cartilage [29], nerve [30], and cardiac [31] tissue repair.

Fetal bovine serum (FBS) is frequently utilized as a supplement for promoting growth in cell and tissue culture media. FBS is beneficial to most human and animal cell types due to its rich source of essential components needed for cell attachment, development, and proliferation [32, 33]. FBS is a sterile liquid obtained from clotted blood collected from pregnant cows and contains various components vital for the growth and survival of mammalian cell lines *in vitro*. Despite the availability of standardized serum-free media, FBS remains the most widely used additive in cell culture media [34]. FBS effectively stimulated fibroblast migration and proliferation *in vitro*, suggesting its promising use in wound repair applications [35]. The present work investigated the efficacy of graphene oxide/chitosan (GO-CTS) nanosheets with and without FBS for regeneration of skin wounds in rats.

Materials and methods

This study includes the fabrication and characterization of the nanocomposite, *in vitro* cytotoxicity testing, and *in vivo* testing of the developed material in a rat model. Rats were received from the House of Experimental Animals, Veterinary Teaching Hospital, Faculty of Veterinary Medicine, Assiut University, Assiut, Egypt. The Assiut Veterinary Medicine Research Ethics Committee, Assiut University, Assiut, Egypt, approved the various steps of the experimental work (No. 06/2024/0264) in compliance with ARRIVE regulations and OIE standards for the care and use of animals in research and education.

Chemicals

Natural graphite powder (20 + 84 mesh, 99.9%) was supplied by Alfa Aesar (Great Britain). Potassium permanganate (KMnO₄), chitosan (CTS, 75% deacetylated), and sodium nitrate were supplied by Sigma Aldrich (Germany). Sulfuric acid (60%) was purchased for Al-Naser Co. (Egypt).

Synthesis of GO-CTS nanocomposite

Graphene oxide was synthesized via Hummer's method [36] based on the strong oxidation of natural graphite, as detailed in previous work by Ibrahim, Abdelhamid [37]. Briefly, 1 g of natural graphite was added into a flask surrounded with an ice bath containing sodium chloride and exposed to magnetic stirring. Subsequently, 10 mL of nitric acid (69–72%) containing 0.5 g sodium nitrate was added to the flask. Sulfuric acid (15 mL, 96.0%) and potassium permanganate (3 g, 99%) were incrementally introduced into the mixture. The temperature was maintained below 0 °C via an ice-sodium chloride bath. Following 2 h of magnetic stirring, 200 mL of distilled water was gradually added to the mixture, resulting in a dark brown colloidal suspension. Hydrogen peroxide (30–32%, 15 mL) was added to eliminate the surplus permanganate

until effervescence ceased. Following additional stirring for 30 min, the mixture was filtered and repeatedly rinsed with a 5 wt% HCl solution to eliminate sulfate ions. GO-CTS material was prepared following Abdelhamid and Wu [38] with modification. Chitosan was dissolved at 1 wt% in water containing 1 wt% acetic acid to prepare the solution. GO (1 wt%) was then added and the solution was stirred overnight till obtaining a homogenous colloidal solution of GO-CTS.

Characterization instruments

X-ray diffraction (XRD) analysis was conducted using a Bruker AXS D8 Advance System (Germany). The powdered sample was placed on a zero-background holder. Transmission electron microscopic (TEM) imaging for GO was performed on a JEM-2100 TEM (JEOL, Japan). The image was obtained from a diluted dispersion in an aqueous solution. A 10 μ L aliquot of the dispersion was deposited onto a copper grid coated with a carbon film. Fourier transform infrared (FT-IR) spectra were collected on attenuated total reflectance FT-IR (ATR-FTIR) spectra (UK, Varian 610-IR). The sample was analyzed via direct deposition on a diamond piece of the Golden Gate ATR accessory.

Cytotoxicity assay

For mitigating the detrimental effects of leached chemicals, extracts were generated from the GO-CTS nanocomposite. Ethylene oxide gas was used to sterilize the nanomaterials, which were subsequently placed in serum-free Dulbecco's Modified Eagle's Medium (DMEM; Invitrogen, USA) containing 1% penicillin/streptomycin (p/s; Gibco, USA) at 37 °C with shaking at 120 rpm for 72 h. The incubation was conducted with a culture medium at a concentration of 0.2 g/mL [39]. After incubation, the supernatant was collected, centrifuged to obtain conditioned extracts, filtered through 0.4 μ m filters, and preserved at 4 °C for subsequent cytotoxicity analysis.

Human endothelial cells (ECs), specifically the EA.hy926 cell line and mouse embryonic fibroblasts (MEFs), were cultured in DMEM containing 10% fetal bovine serum (Hyclone, USA) and 1% p/s under standard conditions (37 °C, 5% CO₂) in a humidified incubator. Cells were harvested at 70% confluency by trypsinization for further experimental procedures. For the assay, cells were cultured at 1.5×10^4 cells per well in a 48-well plate and incubated for 24 h in complete culture medium (DMEM supplemented with 10% FBS and 1% p/s) to promote adhesion. After aspiration of the medium, 500 μ L of either the conditioned or control medium was placed into each well.

For the control groups, the negative control wells contained cells grown in DMEM containing 1% p/s

(without FBS), whereas the positive control group (toxic group) was treated with 20% dimethyl sulfoxide (DMSO) to induce extensive cell lysis. Additionally, a 10% FBS-treated group was included to assess the effect of serum on cell viability. The extracts' effect on cellular response was assessed after 24 h of incubation using the (3-[4,5-dimethylthiazol-2-yl]-2,5 diphenyl tetrazolium bromide) (MTT) assay. Metabolically active cells convert MTT dye into purple formazan crystals. In brief, 50 μ L of MTT solution (5 mg/mL; Sigma-Aldrich, USA) was introduced to each well, followed by 4 h of incubation at 37 °C. Following incubation, the medium with the MTT dye was discarded, and 250 μ L of DMSO was added. After incubating for 10 min, 100 μ L aliquots were transferred to a 96-well plate, and absorbance was recorded at 570 nm using a spectrophotometer. Cell viability was calculated relative to negative control.

Skin wound healing model induction

In this study, female rats ($n=20$, 8 weeks, 200–250 g) were utilized to assess the efficacy of GO-CTS nanosheets alone or combined with FBS in enhancing the skin healing cascade. Rats were housed individually in standard conditions and provided with a diet of commercial rat chow and *ad libitum* access to water. A 7-day acclimatization period was provided to the animals prior to surgery. The model of skin healing was conducted as described by Soliman, Sadek [2] and Hussein, Abdelhamid [15]. A total of 40 skin defects were placed in a random manner into four groups; the control group, the GO-CTS treated group, the FBS treated group, and the GO-CTS/FBS treated group. Animals were subjected to isoflurane inhalation anesthesia (Forane: AbbVie, England) through the usage of an induction chamber at a dose of 2–3.5% in 100% oxygen for induction and a nose cone at a dose of 1.5–3.5% for maintenance anesthesia. Aseptic preparation of the skin on the dorsum was done, and the animals were placed in sternal recumbency. An 8 mm in diameter circular full-thickness model of skin wounds had been performed bilaterally on the dorsum, with a distance of 2 cm between the wounds. The skin defects were treated with 0.3 mL of saline (control defects), GO-CTS, FBS (0.3 mL), or GO-CTS/FBS. Rats then returned to their boxes and were allowed to move without limitations with careful monitoring for any complications throughout the study. The animals were euthanized on days 7 and 21 after induction of skin wounds via the use of isoflurane followed by decapitation.

Gross evaluation of the wound

The wounds were digitally photographed on days 0, 7, and 21, with a calibrated ruler placed beside the wounds to enable accurate digital measurement of the photos. Wound closure was measured using ImageJ software and

presented as a percentage, following the method previously outlined [2], using the formula below:

$$\text{Wound closure (\%)} = \frac{\text{Initial wound area} - \text{Wound area at each time point}}{\text{Initial wound area}} \times 100$$

Histological examination

The skin tissue samples were obtained then fixed in 10% neutral buffered formalin. After fixation, the samples underwent routine processing, were embedded in paraffin, sectioned, and stained using hematoxylin and eosin. The epithelial gap between the left and right wound edges was measured in micrometers using ImageJ, with five wounds being analyzed per group. The number of inflammatory cells, and the number and average diameter of the new blood vessels were also counted. All histological analyses were performed on five images per wound sample to obtain the statistical results [2, 40].

Histochemical staining of collagen

Gomori's trichrome stain was applied to investigate the wound healing process, highlighting the extent of collagen deposition. The tissue sections embedded in paraffin were first deparaffinized using xylene, then gradually rehydrated through a sequence of ethanol solutions, followed by immersion in phosphate-buffered saline, and

finally rinsed with distilled water. The sections were then stained with Gomori's trichrome stain following the manufacturer's guidelines, dehydrated through a series of alcohol solutions, cleared in xylene, and mounted. Collagen staining with green color was then verified under the microscope. Measurement of granulation tissue thickness was performed on a scale of 1–3: 1 = mild; 2 = moderate; 3 = complete [40]. The percentage of collagen-positive areas was assessed in ImageJ using a threshold area fraction method. Collagen content was quantified as a percentage of the total pixel count in the field of view and reported as the mean \pm standard deviation [41].

Statistical analysis

One-way ANOVA followed by Tukey's post hoc test was conducted for statistical analysis in IBM SPSS software (version 21, USA), and results with a *p*-value less than 0.05 were considered statistically significant.

Results

GO-CTS nanocomposite synthesis and characterization

GO was synthesized via strong oxidation of graphite following Hummer's method. It was then dispersed into a solution of CTS producing GO-CTS biomaterial. The material was analyzed using XRD (Fig. 1A), TEM image (Fig. 1B), and FT-IR spectra (Fig. 1C).

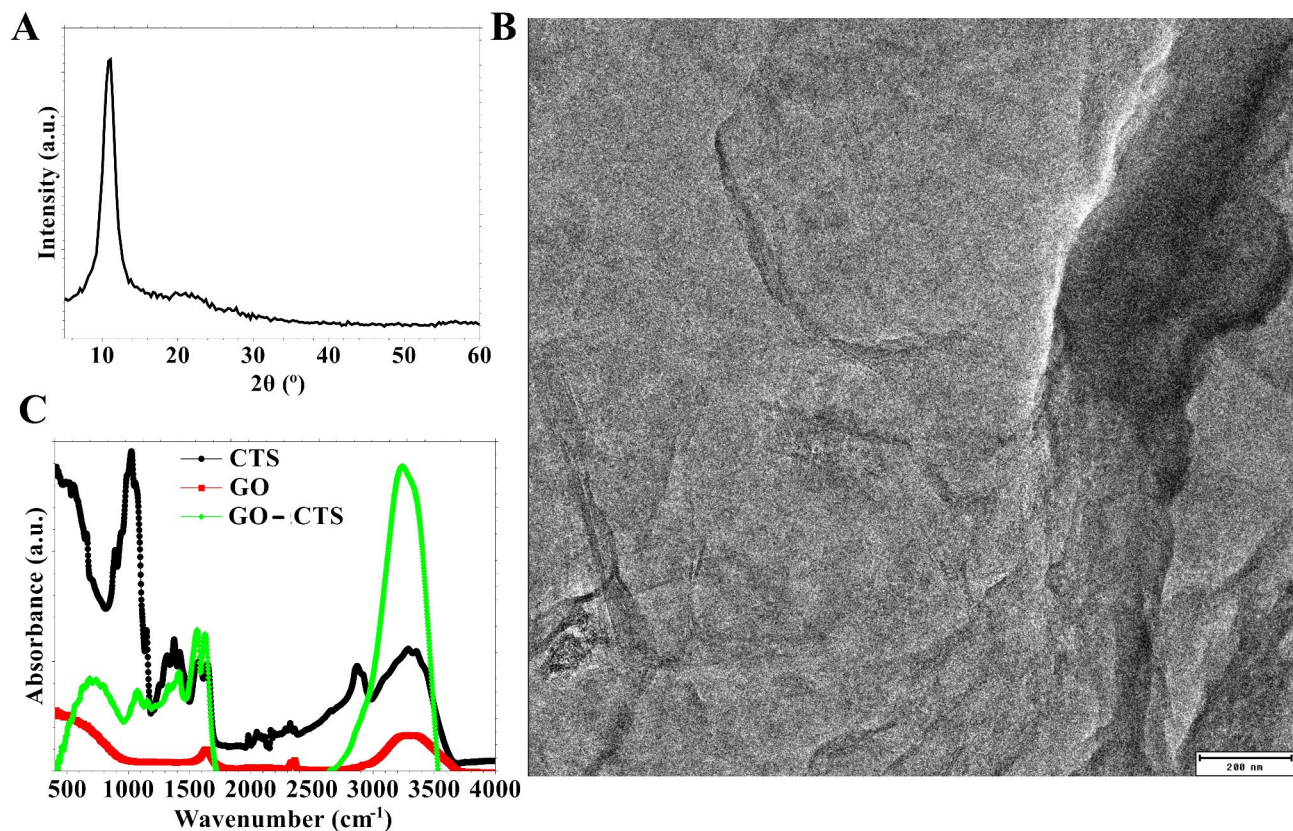


Fig. 1 Characterization of GO-CTS biomaterials using (A) XRD, (B) TEM image, and (C) FT-IR

The phase and material's crystallinity were characterized using XRD (Fig. 1A). The XRD spectrum for GO displays a prominent Bragg diffraction peak at 10.9° , matching the Miller index of the (002) plane. The observed diffraction peaks refer to d-spacing of 0.9 nm. The shape of GO was evaluated using a TEM image (Fig. 1B). The transparency observed in the TEM image of GO suggests that it consists of a few 2D layers. Additionally, the TEM image reveals a crumbling appearance of GO.

The functional groups and interactions inside GO-CTS were determined using FT-IR (Fig. 1C). GO displays vibrational bands at 3280 cm^{-1} , and 1640 cm^{-1} which correspond to O–H stretching, and C=O stretching of carboxylic acid groups. The observed FT-IR peak at 2350 cm^{-1} refers to CO_2 adsorbed into the materials. The FT-IR spectra of CTS exhibit distinctive bands at 3300 cm^{-1} , 2870 cm^{-1} , 1650 , 1560 cm^{-1} , 1380 cm^{-1} , and 1020 cm^{-1} O–H stretching, C–H/ N–H stretching, C=O stretching, N–H bending, $\text{CH}_2\text{-OH}$, and C–O, respectively. GO-CTS composite displays the distinctive FT-IR characteristics peaks for both materials, i.e. GO and CTS. Nevertheless, the vibrational bands of C=O and C–O for CTS show shift in their wavenumber due to the interactions with GO via hydrogen bonds.

Cytotoxicity assay

MTT assay indicated no significant difference in viability between EA.hy926 endothelial cells grown in complete DMEM and those treated with conditioned extracts from the GO-CTS material after 24 h (Fig. 2A). Furthermore, preconditioned media containing GO-CTS and supplemented with FBS demonstrated a higher percentage of cell proliferation compared to other groups. The positive

control group (treated with DMSO) showed a significant reduction in viability at $3.1\% \pm 1.8\%$. Cells exposed to the GO-CTS-containing extracts exhibited a viability of $99.2\% \pm 5.7\%$. Notably, cells treated with FBS alone showed a viability of $109\% \pm 2.5\%$, and those exposed to the combination of GO-CTS and FBS demonstrated the highest viability at $111.8\% \pm 3.9\%$ with no significant difference with the FBS alone.

In the analysis of MEF, the results paralleled the previous findings (Fig. 2B). The negative control group (DMEM) maintained a baseline cell viability set at 100%. The positive control group, treated with DMSO, displayed a significant reduction in cell viability, recorded as $2.4\% \pm 1.2\%$. Cells exposed to GO-CTS demonstrated a viability of $110.5\% \pm 3.9\%$, while cells treated with FBS alone reached $118.2\% \pm 2.1\%$. Importantly, the combination of GO-CTS and FBS yielded the highest cell viability, recorded at $121.4\% \pm 4.4\%$, closely aligned with the endothelial cell findings.

Assessment of the wound closure in vivo

Wounds treated with GO-CTS, FBS, or GO-CTS/FBS exhibited a significantly accelerated healing process compared to the control group. The wound closure was not visibly observed on day 7. However, complete wound closure was observed in GO-CTS, FBS, or GO-CTS/FBS treated groups on day 21 and closure rates were recorded at $85.5\% \pm 0.56\%$, $87.5\% \pm 1.75\%$, or $91.5\% \pm 1.03\%$, respectively (Figs. 3A and B). Among the treatments, GO-CTS/FBS combination demonstrated the most pronounced effect, leading to the fastest closure rate, indicating a synergistic effect of the combined treatment. (Fig. 3B). A notable increase in hair growth was observed in the wound area following treatment with GO-CTS/

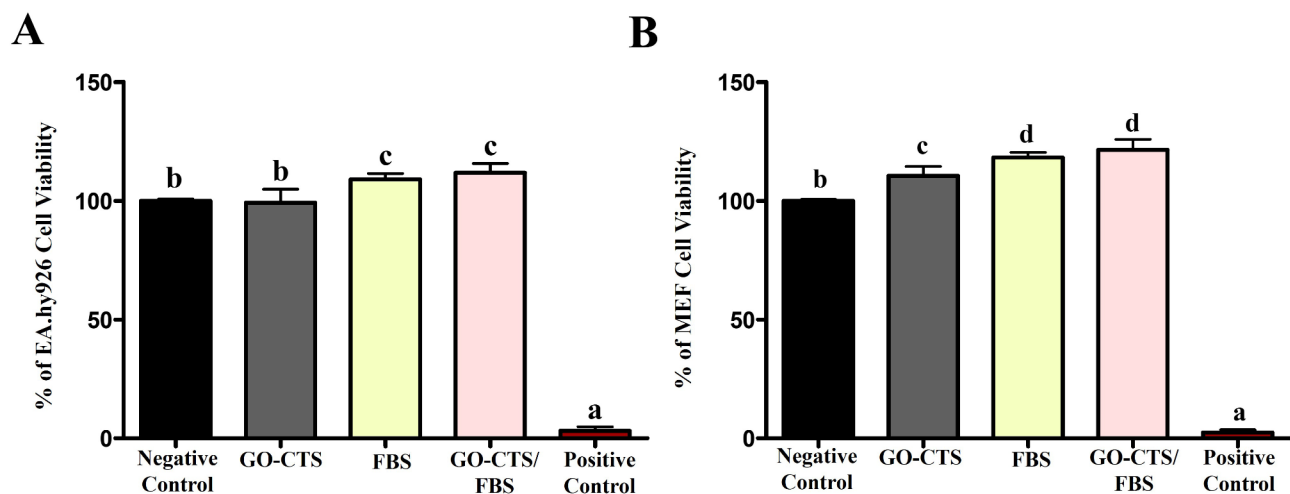


Fig. 2 Cytotoxicity assay in vitro. MTT assay for cell viability of EA.hy926 endothelial cells (A) and MEF (B) cultured using extracts of GO-CTS, FBS, or GO-CTS/FBS for 24 h, compared to the negative control. Error bars represent the means \pm standard deviation ($n=8$ for each time point), with differences assessed using one-way ANOVA followed by Tukey's HSD post hoc test. Groups marked with different letters represent statistically significant differences ($p < 0.05$), whereas groups sharing the same letter show no significant difference. The assay was done in triplicate

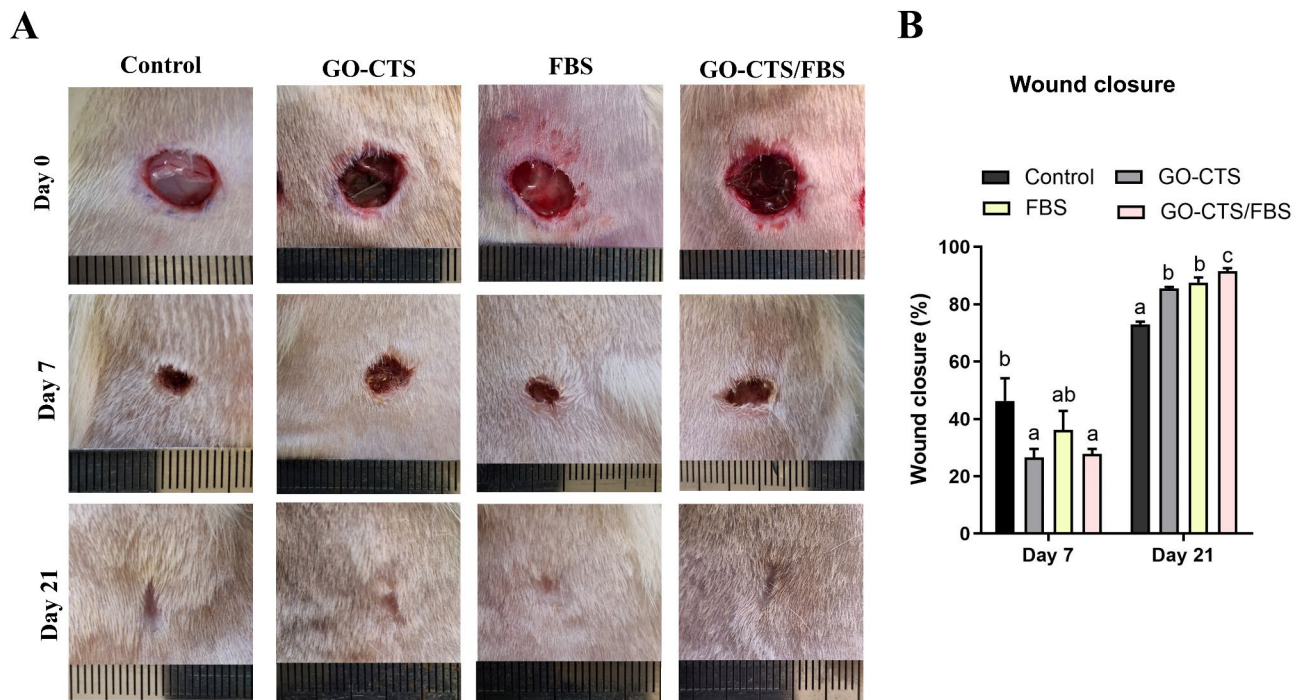


Fig. 3 Gross assessment of skin wounds treated with or without GO-CTS, FBS, or GO-CTS/FBS. **(A)** Images showing skin wounds from the control and treated groups at days 0, 7, and 21. **(B)** Wound closure was quantified as a percentage through ImageJ analysis. Groups labeled with different letters represent statistically significant differences ($p < 0.05$), whereas groups sharing the same letter show no significant difference. Differences were evaluated using one-way ANOVA followed by Tukey's HSD post hoc test

FBS (Fig. 3A). These findings highlight the effectiveness of GO-CTS, FBS, and particularly their combination in enhancing wound healing and tissue regeneration.

Histological findings on re-epithelization, inflammation and angiogenesis

To monitor the healing process, histological evaluations of the wounds were carried out on days 7 and 21. This involves assessing various aspects including re-epithelialization, inflammation, and angiogenesis.

Re-epithelialization was assessed by measuring the epithelial gap between the growing epidermis at the wound edges. By day 7, no significant difference was observed between the control and treated groups. (Figure 4A A). However, it was significantly enhanced following treatment with GO-CTS, FBS, or GO-CTS/FBS, as evidenced by a reduction in the epithelial gap by day 21 (Fig. 4A A). Notably, the GO-CTS/FBS-treated wounds exhibited complete re-epithelialization, forming a well-structured epithelial layer with evidence of skin appendage regeneration (such as the formation of hair follicles and sebaceous glands). In contrast, the epithelial layers in the GO-CTS and FBS groups appeared thin and incomplete, lacking the fully developed four-strata architecture. The control group displayed incomplete wound healing, with a persistent epithelial gap and delayed tissue regeneration (Fig. 4A).

Analysis of inflammatory cell infiltration revealed an initial influx of inflammatory cells into the wound area in the GO-CTS and GO-CTS/FBS groups on day 7, while the FBS group showed no significant inflammatory response (Figs. 4B and 5B). By day 21, the number of inflammatory cells had decreased significantly in all treated groups, indicating resolution of inflammation and progression of tissue remodeling (Figs. 4B and 5B). However, the control group showed a persistent presence of inflammatory cells, indicating delayed healing (Fig. 5B).

Angiogenesis was significantly enhanced in the treated groups by day 7 as the number of the newly formed blood vessels was markedly increased in the GO-CTS, FBS, and GO-CTS/FBS groups compared to the control group (Fig. 5C). Additionally, blood vessel size was significantly increased in the GO-CTS and GO-CTS/FBS groups, but not in the FBS-treated wounds (Fig. 5D).

However, by day 21, the number and size of newly formed blood vessels was significantly decreased in the treated wounds (Fig. 5C and D), whereas the control group showed a notable increase in blood vessel number and size (Fig. 5C and D). These findings suggest that GO-CTS and FBS promote the early proliferative phase of wound healing by stimulating angiogenesis.

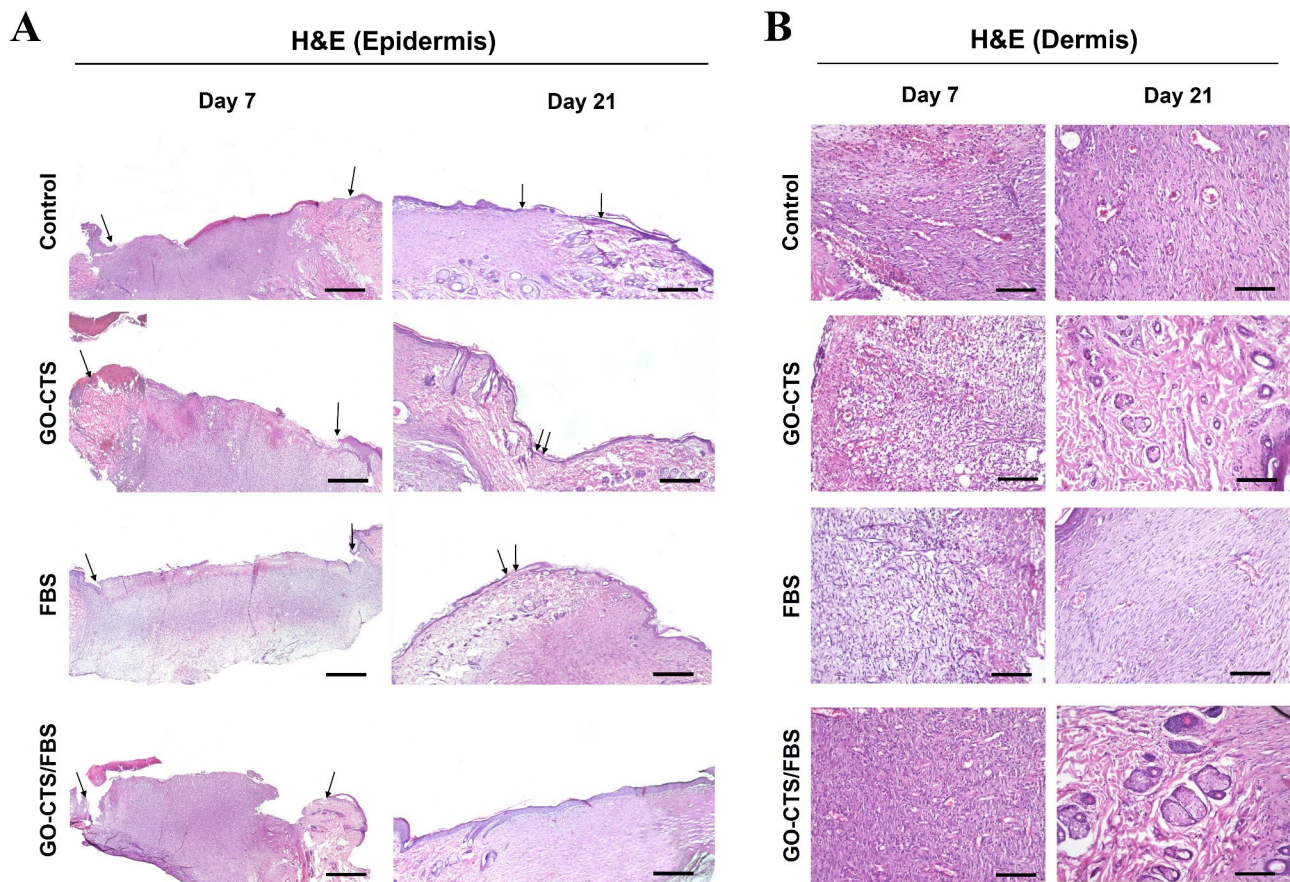


Fig. 4 Histological evaluation of skin wounds in rats treated with or without GO-CTS, FBS, or GO-CTS/FBS. **(A)** and **(B)** Wound sections from control or GO-CTS, FBS, or GO-CTS/FBS-treated wounds collected on days 7 and 21 and stained by Hematoxylin and Eosin. Arrows highlight the epithelial layer. In **(A)**, the scale bar measures 100 μm , and in **(B)**, it measures 50 μm

Histological evaluation of the granulation tissue

Gomori's trichrome staining was applied to the wound sections to assess and quantify collagen deposition and granulation tissue formation at the wound center. On day 7 post-wounding, granulation tissue thickness showed no significant differences among the GO-CTS, FBS, GO-CTS/FBS groups, and the control group. At day 21 post-wounding, the GO-CTS, FBS, and GO-CTS/FBS groups displayed notably thick and well-formed granulation tissue (Fig. 6A–C) and higher amounts of collagen content with a dense arrangement and staining of collagen fibers, in comparison to the control group (Fig. 6D).

Discussion

Skin wounds with an impaired healing process are a significant health issue with considerable life and economic consequences. In recent decades, skin tissue engineering has aimed to overcome complications of non-healing wounds. Consequently, various scaffold materials have been explored to support and induce regeneration [2, 10, 11, 42]. Among these, GO and CTS have gained attention in tissue engineering due to their unique properties,

including biocompatibility and the ability to promote cell migration, adhesion, and proliferation [2, 42–44]. When GO is combined with other compounds such as cellulose, it forms a composite material with the potential to enhance wound healing [2, 15, 18]. Additionally, CTS integrated into nanocomposites with materials such as fucoidan, pullulan, and gallium, has been shown to stimulate the process of wound healing [42, 44].

The synthesis and characterization of GO and its composite with CTS yield significant insights into the structural and functional attributes of the GO-CTS biomaterial. The findings from XRD (Fig. 1A), TEM (Fig. 1B), and FT-IR (Fig. 1C) investigations collectively validate the effective synthesis of GO, its incorporation with CTS, and the creation of a GO-CTS composite.

The XRD investigation exhibited a significant Bragg diffraction peak at 10.9° , corresponding to the (002) plane of GO, aligning with prior results that confirm the effective oxidation of graphite (Fig. 1A). The determined d-spacing of 0.9 nm signifies the incorporation of oxygen-containing functional groups during the oxidation process, a characteristic feature of GO synthesis. The interlayer

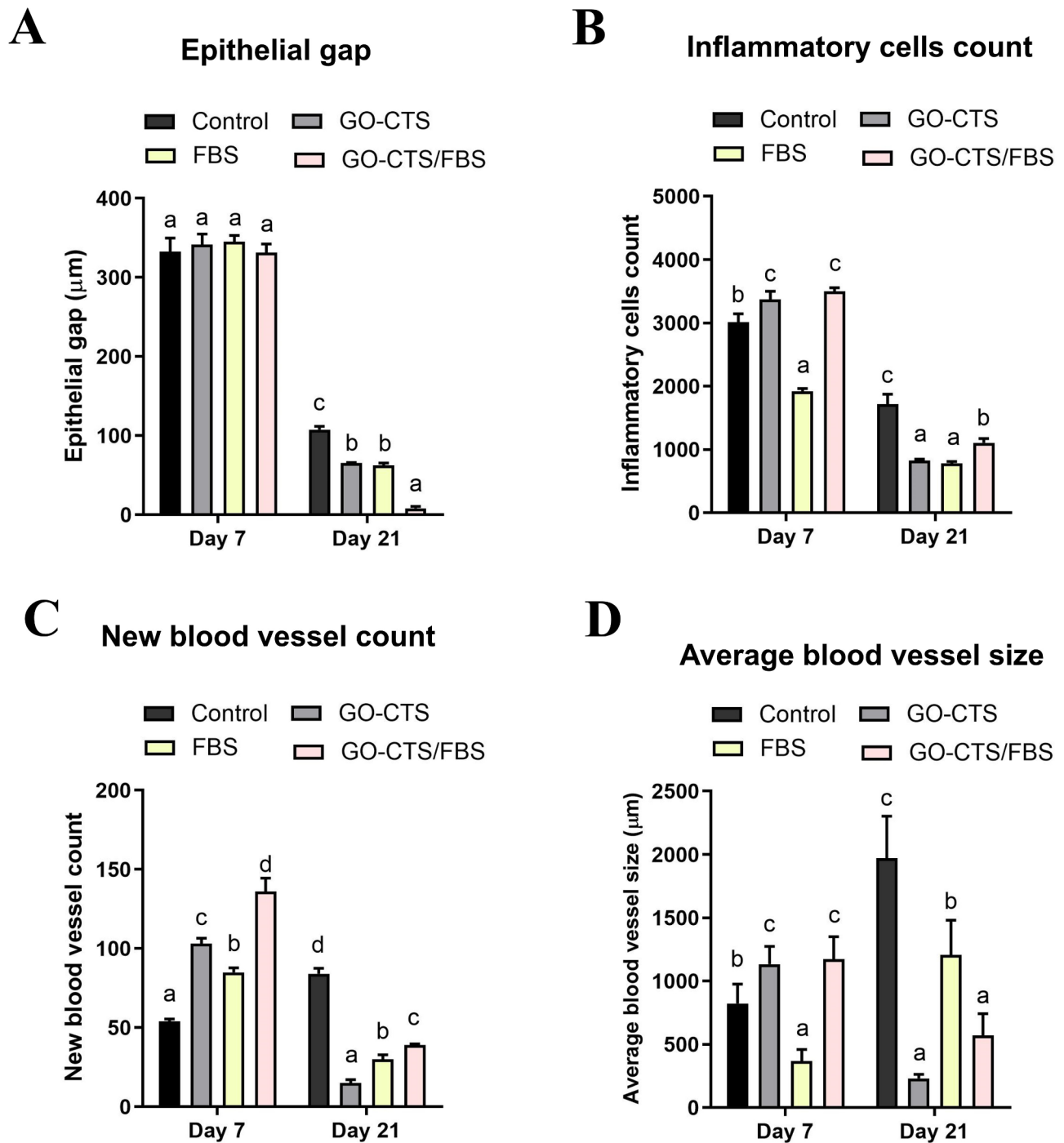


Fig. 5 Histomorphometric analysis of the newly formed tissue in vivo. **(A)** The epithelial gap between the two wound edges as well as **(B)** the count of inflammatory cells at the wound site were quantified using ImageJ. **(C)** The number of new blood vessels was quantified in 5 images per section. **(D)** The size of the new blood vessels was assessed with ImageJ. Groups marked with different letters represent statistically significant differences ($p < 0.05$), whereas groups sharing the same letter show no significant difference. Differences were evaluated using one-way ANOVA followed by Tukey's HSD post hoc test

spacing relative to pure graphite (about ~0.34 nm) is ascribed to the presence of these functional groups, which concurrently improve the material's hydrophilicity and dispersibility in aqueous conditions [14].

The TEM image further substantiates the development of GO, exhibiting a few-layered two-dimensional structure characterized by a translucent and crumpled appearance (Fig. 1B). This morphology is typical of GO sheets. The deformed structure indicates the existence of

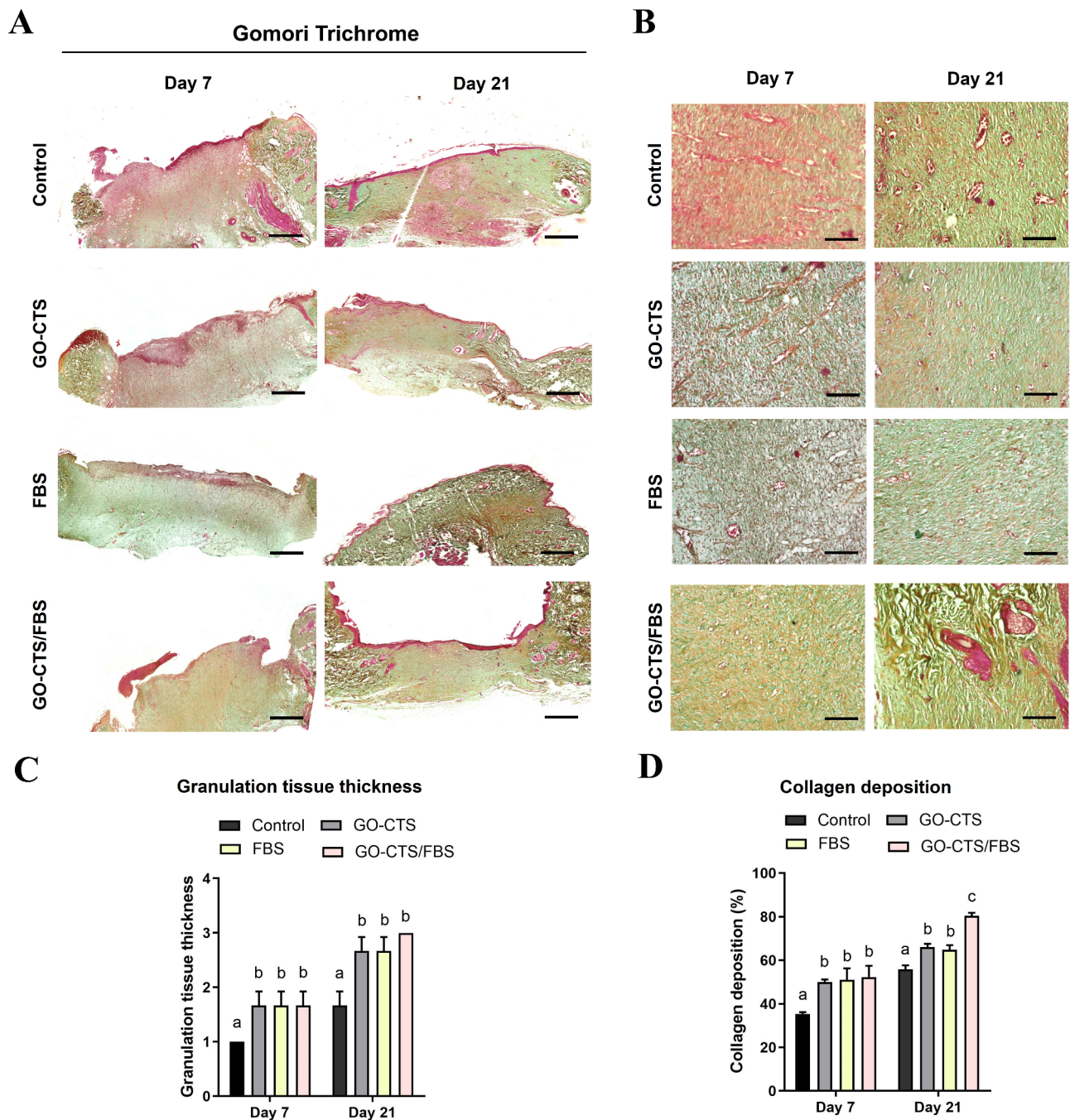


Fig. 6 Histochemical evaluation of skin wounds in rats treated with or without GO-CTS, FBS, or GO-CTS/FBS. **(A)** and **(B)** Gomori's Trichrome stained skin sections from control and GO cellulose-treated wounds obtained on days 7 and 21. In image **(A)**, the scale bar is 100 μ m, and in image **(B)**, it is 50 μ m. **(C)** Granulation tissue thickness was assessed using a scale of 1–3, as mentioned in the Materials and Methods. **(D)** Collagen deposition was quantified using ImageJ. Bars sharing the same letter indicate values that are not significantly different. Differences were evaluated using one-way ANOVA followed by Tukey's HSD post hoc test

flaws and functional groups, which are crucial for interactions with other materials, such as CTS, in composite synthesis.

The FT-IR spectra offer essential insights into the functional groups present in GO, CTS, and the GO-CTS composite (Fig. 1C). The vibrational bands detected for

GO, including O–H stretching (3280 cm^{-1}) and C=O stretching (1640 cm^{-1}), validate the existence of hydroxyl and carboxyl groups, which are incorporated during the oxidation process. These functional groups enhance the material's hydrophilicity and promote its contact with CTS via hydrogen bonding and electrostatic interactions

[16]. The FT-IR spectra of CTS display distinctive peaks associated with O–H stretching, C–H/N–H stretching, and C=O stretching, among others, aligning with its polysaccharide structure. The FT-IR analysis of the GO-CTS composite confirms the successful conjugation of GO and CTS, as indicated by the existence of distinctive peaks from both substances. The alterations in the vibrational bands of C=O and C–O in CTS indicate the establishment of hydrogen bonds between GO and CTS.

The results of XRD, FT-IR, and TEM image validate the effective synthesis of GO and its incorporation with CTS to create a GO-CTS composite. The identified structural and functional characteristics, including the enhanced d-spacing, crumpled morphology, and hydrogen bonding interactions, underscore the potential of this biomaterial for diverse biomedical applications, such as wound healing.

Furthermore, FBS is widely utilized as a supplement in cell culture media due to its abundance of growth factors, hormones, and nutrients crucial for promoting cell growth and proliferation [32, 45, 46]. While FBS is primarily used *in vitro*, there is limited evidence of its potential role in accelerating wound healing *in vivo*. Therefore, this study investigated the effects of GO-CTS and FBS on wound healing. We demonstrated that GO-CTS with FBS is a promising composite that significantly improves wound healing in a full-thickness skin wound model *in vivo*.

Cytocompatibility is crucial for skin tissue engineering to ensure that biomaterials support *in vivo* fibroblast and endothelial cell growth and adhesion [15]. Here, the cytotoxicity of the designed materials was tested on human ECs and MEF cells. The results indicated that the materials are cytocompatible, which is consistent with previous studies [2, 15, 47–49].

The ability of these biomaterials to promote regeneration depends on the host's cellular reaction to the implanted materials, which triggers the influx of various immune cells [50]. The early recruitment of inflammatory cells, notably neutrophils and macrophages, plays a key role in wound cleaning and debris removal. Subsequently, during the proliferative and remodeling phases, macrophages promote angiogenesis, fibroblast proliferation, and collagen matrix deposition. As healing progresses, the number of inflammatory cells decreases due to an increase in fibroblasts [2, 51]. Aligned with this, our findings on day 7 displayed inflammatory cell infiltration in the wounds treated with GO-CTS and GO-CTS/FBS.

Neovascularization is a vital aspect in wound healing, as it supplies essential nutrients and oxygen to the healing tissue while removing waste products and promoting granulation tissue formation. It arises from pre-existing blood vessels through mechanisms driven by growth factors, inflammatory mediators, and extracellular matrix

remodeling [52]. Our study suggests that GO-CTS and FBS enhance wound healing by promoting blood vessel formation, as reflected by a greater number of newly formed blood vessels in the early proliferation phase and larger vessel diameters in the later stages of the healing process.

Collagen, primarily synthesized by fibroblasts, serves as the key extracellular matrix component necessary for granulation tissue formation and the remodeling phase of wound healing [4, 53, 54]. In our study, collagen formation was minimal during the early phase of healing process, as the wounds were transitioning from inflammation to proliferation. As healing progressed, collagen became more mature and densely packed, and normal skin structures began to reappear. These observations suggest that treatment with GO-CTS and FBS may promote more efficient wound healing by enhancing granulation tissue formation and organization and collagen deposition. Moreover, the synergistic effect of GO-CTS and FBS ultimately leads to better tissue repair and regeneration compared to GO-CTS or FBS alone.

The favorable microenvironment created by GO-CTS and FBS in this study likely expedited wound closure and minimized the epithelial gap between wound edges. Inflammatory cell infiltration in the wound area stimulates the release of chemotactic and growth factors, initiating the proliferation of cells necessary for healing [50, 51, 53]. GO and CTS demonstrated immunomodulatory effects, promoting the migration of inflammatory cells that produce interleukin-1 (IL-1), IL-6, IL-8, platelet-derived growth factor (PDGF), transforming growth factor- β (TGF- β), and vascular endothelial growth factor (VEGF). These factors are critical in promoting healing cascades, including neovascularization, fibroblast proliferation, and collagen deposition [2, 12, 50, 55, 56]. Additionally, the surface properties and chemical composition of the GO-CTS material may enhance cell adhesion, proliferation, and migration [12, 15, 57]. FBS contains a variety of cytokines and growth factors that stimulate cell proliferation, migration, and differentiation, contributing to the tissue repair. These key factors include epidermal growth factor, fibroblast growth factor, insulin-like growth factor, PDGF, TGF- β , and IL-1, -2, -4, -6, -8, and -10 [50, 58]. All these factors promote the migration and proliferation of epithelial cells from the wound edges across the remaining basement membrane of the skin wound [53, 54].

Conclusion

GO-CTS is a biocompatible nanocomposite capable of supporting the *in vitro* growth of fibroblasts and endothelial cells. Moreover, the *in vivo* application of GO-CTS, with or without the addition of FBS, significantly enhances the healing process of full-thickness skin

wounds in a rat model. These findings could contribute to the development of a fast and effective wound healing agent for clinical use.

However, this experimental study has certain limitations, including the lack of assessment of material biodegradation, a small in vivo sample size, and insufficient investigation of the possible cellular and molecular mechanisms underlying the material's stimulatory effects. Therefore, future research should focus on evaluating the biodegradation of the GO-CTS nanocomposite as a scaffold for skin tissue regeneration. Additionally, the in vivo fate of its degradation byproducts must be assessed. Further studies should also be conducted on a larger sample size and animal models, including different skin wound types such as burn injuries and wounds in diabetic animals.

Abbreviations

CTS	Chitosan
DMSO	Dimethyl sulfoxide
DMEM	Dulbecco's Modified Eagle's Medium
MEFs	Embryonic fibroblasts
FBS	Fetal bovine serum
GO	Graphene oxide
GO-CTS	Graphene oxide chitosan
ECs	Human endothelial cells
IL	Interleukin
PDGF	Platelet derived growth factor
TGF- β	Transforming growth factor- β

Acknowledgements

NA.

Author contributions

Conceptualization: KHH and AAS; Data Curation: KHH, MS, MSS, HNA, MA, AAS; Investigation: KHH and AAS; Methodology: KHH, MS, MSS, HNA, MA, AAS; Supervision: KHH; Validation: KHH and AAS; Writing-Original Draft Preparation: KHH, MS, MSS, HNA, MA, AAS; Writing-Review and Editing: KHH, MS, MSS, HNA, AAS.

Funding

Open access funding provided by The Science, Technology & Innovation Funding Authority (STDF) in cooperation with The Egyptian Knowledge Bank (EKB).

The authors declare that no specific funding was received for this study.

Data availability

No datasets were generated or analysed during the current study.

Declarations

Ethics approval and consent to participate

The Assiut Veterinary Medicine Research Ethics Committee, Assiut University, Assiut, Egypt, approved the various steps of the experimental work (No. 06/2024/0264) in compliance with ARRIVE regulations and OIE standards for the care and use of animals in research and education. Rats were received from the House of Experimental Animals, Veterinary Teaching Hospital, Faculty of Veterinary Medicine, Assiut University, Assiut, Egypt. As the animals were sourced from an institutional facility, no additional informed consent was required.

Consent for publication

All authors have approved the final version of the manuscript.

Competing interests

The authors declare no competing interests.

Author details

¹Department of Surgery, Anesthesiology and Radiology, Faculty of Veterinary Medicine, Assiut University, Assiut 71516, Egypt

²Tissue Culture and Stem Cells Unit, Molecular Biology Researches & Studies Institute, Assiut University, Assiut 71526, Egypt

³Department of Pathology and Clinical Pathology, Faculty of Veterinary Medicine, Assiut University, Assiut 71516, Egypt

⁴Department of Pharmacology, Faculty of Veterinary Medicine, Assiut University, Assiut 71516, Egypt

⁵Department of Chemistry, Faculty of Science, Imam Mohammad Ibn Saud Islamic University (IMSIU), Riyadh 11623, Saudi Arabia

⁶Department of Cell and Tissues, Faculty of Veterinary Medicine, Assiut University, Assiut 71526, Egypt

Received: 5 December 2024 / Accepted: 28 March 2025

Published online: 07 May 2025

References

- Lin Y, Chen Z, Liu Y, Wang J, Lv W, Peng R. Recent advances in nano-formulations for skin wound repair applications. *Drug Des Devel Ther.* 2022;16:2707–28. <https://doi.org/10.2147/DDDT.S375541>
- Soliman M, Sadek AA, Abdelhamid HN, Hussein K. Graphene oxide-cellulose nanocomposite accelerates skin wound healing. *Res J Vet Sci.* 2021;137:262–73.
- Pavletic MM. Atlas of small animal wound management and reconstructive surgery. Wiley; 2018.
- Lux CN. Wound healing in animals: a review of physiology and clinical evaluation. *Vet Dermatol.* 2022;33(1):91–e27.
- Basu S, Shukla V. Complications of wound healing. In: Mani R, Romanelli M, Shukla V, editors. Measurements in wound healing: science and practice. London: Springer London; 2013. pp. 109–44.
- Das S, Baker AB. Biomaterials and nanotherapeutics for enhancing skin wound healing. *Front Bioeng Biotechnol.* 2016;4.
- Yang F, Bai X, Dai X, Li Y. The biological processes during wound healing. *Regen Med.* 2021;16(04):373–90.
- Yang J, Jing X, Wang Z, Liu X, Zhu X, Lei T, et al. In vitro and in vivo study on an injectable glycol chitosan/dibenzaldehyde-terminated polyethylene glycol hydrogel in repairing articular cartilage defects. *Front Bioeng Biotechnol.* 2021;9:607709.
- Le LT, Giang NN, Chien PN, Trinh XT, Long NV, LT VANA, et al. Enhancement of wound healing efficacy by chitosan-based hydrocolloid on sprague dawley rats. *IV.* 2023;37(3):1052–64.
- Chen J, Fan Y, Dong G, Zhou H, Du R, Tang X, et al. Designing biomimetic scaffolds for skin tissue engineering. *Biomater Sci.* 2023;11(9):3051–76.
- Sierra-Sánchez Á, Kim KH, Blasco-Morente G, Arias-Santiago S. Cellular human tissue-engineered skin substitutes investigated for deep and difficult to heal injuries. *NPJ Regen Med.* 2021;6(1):35.
- Kim Y, Zharkinbekov Z, Razyieva K, Tabyldiyeva L, Berikova K, Zhumagul D et al. Chitosan-based biomaterials for tissue regeneration. *Pharm.* 2023;15(3).
- Sadek AA, Abd-Elkareem M, Abdelhamid HN, Moustafa S, Hussein K. Repair of critical-sized bone defects in rabbit femurs using graphitic carbon nitride (g-C₃N₄) and graphene oxide (GO) nanomaterials. *Sci Rep.* 2023;13(1):5404.
- Abdelhamid HN, Khan MS, Wu H-F. Graphene oxide as a nanocarrier for gramicidin (GOGD) for high antibacterial performance. *RSC Adv.* 2014;4(91):50035–46.
- Hussein KH, Abdelhamid HN, Zou X, Woo HM. Ultrasonicated graphene oxide enhances bone and skin wound regeneration. *Mater Sci Eng C Mater Biol Appl.* 2019;94:484–92.
- Abdelhamid HN, Wu H-F. Synthesis of a highly dispersive sinapinic Acid@graphene oxide (SA@GO) and its applications as a novel surface assisted laser desorption/ionization mass spectrometry for proteomics and pathogenic bacteria biosensing. *Anlst.* 2015;140(5):1555–65.
- Abdelhamid HN. An introductory review on advanced multifunctional materials. *Heliyon.* 2023;9(7).
- Shanmugam DK, Madhavan Y, Manimaran A, Kiliaraj GS, Mohanraj KG, Kandhasamy N, et al. Efficacy of graphene-based nanocomposite gels as a promising wound healing biomaterial. *Gels.* 2023;9(1):22.
- Gong M, Sun J, Liu G, Li L, Wu S, Xiang Z. Graphene oxide-modified 3D acellular cartilage extracellular matrix scaffold for cartilage regeneration. *Mater Sci Eng C.* 2021;119:111603.

20. Kang MS, Kang JI, Le Thi P, Park KM, Hong SW, Choi YS, et al. Three-dimensional printable gelatin hydrogels incorporating graphene oxide to enable spontaneous myogenic differentiation. *ACS Macro Lett.* 2021;10(4):426–32.
21. Magaz A, Li X, Gough JE, Blaker JJ. Graphene oxide and electroactive reduced graphene oxide-based composite fibrous scaffolds for engineering excitable nerve tissue. *Mater Sci Eng C.* 2021;119:111632.
22. Shahnawaz Khan M, Abdelhamid HN, Wu H-F. Near infrared (NIR) laser mediated surface activation of graphene oxide nanoflakes for efficient antibacterial, antifungal and wound healing treatment. *Colloids Surf B Biointerfaces.* 2015;127:281–91.
23. Hassen A, Moawed EA, Bahy R, El Basaty AB, El-Sayed S, Ali AI, et al. Synergistic effects of thermally reduced graphene oxide/zinc oxide composite material on microbial infection for wound healing applications. *Sci Rep.* 2024;14(1):22942.
24. Nicolle L, Journot CM, Gerber-Lemaire S. Chitosan functionalization: covalent and non-covalent interactions and their characterization. *Polym.* 2021;13(23):4118.
25. Pandey N, Bohra BS, Tiwari H, Pal M, Negi PB, Dandapat A, et al. Development of biodegradable chitosan/graphene oxide nanocomposite via spray drying method for drug loading and delivery application. *J Drug Deliv Technol.* 2022;74:103555.
26. Li H, Zhou X, Luo L, Ding Q, Tang S. Bio-orthogonally crosslinked catechol-chitosan hydrogel for effective hemostasis and wound healing. *Carbohydr Polym.* 2022;281:119039.
27. Sheir MM, Nasra MMA, Abdallah OY. Chitosan alginate nanoparticles as a platform for the treatment of diabetic and non-diabetic pressure ulcers: formulation and in vitro/in vivo evaluation. *Int J Pharm.* 2021;607:120963.
28. Lavanya K, Chandran SV, Balagangadharan K, Selvamurugan N. Temperature- and pH-responsive chitosan-based injectable hydrogels for bone tissue engineering. *Mater Sci Eng C.* 2020;111:110862.
29. Shen Y, Xu Y, Yi B, Wang X, Tang H, Chen C, et al. Engineering a highly biomimetic chitosan-based cartilage scaffold by using short fibers and a cartilage-decellularized matrix. *Biomacromolecules.* 2021;22(5):2284–97.
30. Cheng R, Cao Y, Yan Y, Shen Z, Zhao Y, Zhang Y, et al. Fabrication and characterization of chitosan-based composite scaffolds for neural tissue engineering. *Int J Polym Mater.* 2022;71(11):831–41.
31. Doméngé O, Ragot H, Deloux R, Crépet A, Revet G, Boitard SE, et al. Efficacy of epicardial implantation of acellular chitosan hydrogels in ischemic and nonischemic heart failure: impact of the acetylation degree of chitosan. *Acta Biomater.* 2021;119:125–39.
32. Van der Valk J, Bieback K, Buta C, Cochrane B, Dirks W, Fu J, et al. Fetal bovine serum (FBS): past–present–future. *Altex.* 2018;35(1):1–20.
33. Liu S, Yang W, Li Y, Sun C. Fetal bovine serum, an important factor affecting the reproducibility of cell experiments. *Sci Rep.* 2023;13(1):1942.
34. Wang Y, Wang B, Fu L, Zhou Y. Effect of fetal bovine serum on osteoclast formation in vitro. *Hard Tissue Biol.* 2014;23(3):303–8.
35. Cheng N-C, Tu Y-K, Lee N-H, Young T-H. Influence of human platelet lysate on extracellular matrix deposition and cellular characteristics in adipose-derived stem cell sheets. *Front Cell Dev Biol.* 2020;8:558354.
36. Hummers WS Jr, Offeman RE. Preparation of graphitic oxide. *J Am Chem Soc.* 1958;80(6):1339.
37. Ibrahim M, Abdelhamid HN, Abuelftooh AM, Mohamed SG, Wen Z, Sun X. Covalent organic frameworks (COFs)-derived nitrogen-doped carbon/reduced graphene oxide nanocomposite as electrodes materials for supercapacitors. *J Energy Storage.* 2022;55:105375.
38. Abdelhamid HN, Wu H-F. Multifunctional graphene magnetic nanosheet decorated with chitosan for highly sensitive detection of pathogenic bacteria. *J Mater Chem B.* 2013;1(32):3950–61.
39. Hussein KH, Park K-M, Kang K-S, Woo H-M. Biocompatibility evaluation of tissue-engineered decellularized scaffolds for biomedical application. *Mater Sci Eng C.* 2016;67:766–78.
40. Tan WS, Arulselvan P, Ng SF, Mat Taib CN, Sarian MN, Fakurazi S. Improvement of diabetic wound healing by topical application of vicenin-2 hydrocolloid film on Sprague Dawley rats. *BMC Complement Altern Med.* 2019;19(1):20.
41. Cheng KY, Lin ZH, Cheng YP, Chiu HY, Yeh NL, Wu TK, et al. Wound healing in streptozotocin-induced diabetic rats using atmospheric-pressure argon plasma jet. *Sci Rep.* 2018;8(1):12214.
42. Younas A, Dong Z, Hou Z, Asad M, Li M, Zhang N. A chitosan/fucoidan nanoparticle-loaded pullulan microneedle patch for differential drug release to promote wound healing. *Carbohydr Polym.* 2023;306:120593.
43. Abdelhamid H, Hussein K. Graphene oxide as a carrier for drug delivery of methotrexate. *Biointerface Res Appl Chem.* 2021;11:14726–35.
44. Jiang F, Duan Y, Li Q, Li X, Li Y, Wang Y, et al. Insect chitosan/pullulan/gallium photo-crosslinking hydrogels with multiple bioactivities promote MRSA-infected wound healing. *Carbohydr Polym.* 2024;334:122045.
45. Subbiahanadar Chelladurai K, Selvan Christyraj JD, Rajagopalan K, Yesudhasan BV, Venkatachalam S, Mohan M, et al. Alternative to FBS in animal cell culture - an overview and future perspective. *Heliyon.* 2021;7(8):e07686.
46. Yao T, Asayama Y. Animal-cell culture media: history, characteristics, and current issues. *Reprod Med Biol.* 2017;16(2):99–117.
47. Di Santo MC, Alaimo A, Acebedo SL, Spagnuolo C, Pozner R, Pérez OE. Biological responses induced by high molecular weight chitosan administrated jointly with platelet-derived growth factors in different mammalian cell lines. *Int J Biol Macromol.* 2020;158:953–67.
48. Kumar S, Koh J. Physicochemical, optical and biological activity of chitosan-chromone derivative for biomedical applications. *Int J Mol Sci.* 2012;13(5):6102–16.
49. Vochița G, Cadinoiu AN, Rață D-M, Atanase LI, Popa M, Mahdieh A, et al. Comparative in vitro study between biocompatible chitosan-based magnetic nanocapsules and liposome formulations with potential application in anti-inflammatory therapy. *Int J Mol Sci.* 2024;25(15):8454.
50. Tavakoli S, Kisiel MA, Biedermann T, Klar AS. Immunomodulation of skin repair: cell-based therapeutic strategies for skin replacement (A comprehensive review). *Biomedicines.* 2022;10(1).
51. Wang Z, Qi F, Luo H, Xu G, Wang D. Inflammatory microenvironment of skin wounds. *Front Immunol.* 2022;13.
52. Thittamaranahalli Muguregowda H, Pramod K, Echalasara Govindarama Padmanabha U, Sudesh K, Udaya K, Pragna R. Role of angiogenesis and angiogenic factors in acute and chronic wound healing. *Plast Aesthet Res.* 2015;2:243–9.
53. Ackermann MR. Pathologic Basis of Veterinary Disease. In: F.Zachary J, editor. *Veterinary Dermatology.* 28. 6th ed 2017. pp. 73–131.
54. Wang PH, Huang BS, Horng HC, Yeh CC, Chen YJ. Wound healing. *J Chin Med Assoc.* 2018;81(2):94–101.
55. Feng P, Luo Y, Ke C, Qiu H, Wang W, Zhu Y et al. Chitosan-based functional materials for skin wound repair: mechanisms and applications. *Front Bioeng Biotechnol.* 2021;9.
56. Motiea E, Hussein MT, Hussein KH. Investigating the healing potential of fresh amniotic membranes in full-thickness canine skin wounds. *Assiut Veterinary Med J.* 2025;71(184):73–80.
57. Sahana TG, Rekha PD. Biopolymers: applications in wound healing and skin tissue engineering. *Mol Biol Rep.* 2018;45(6):2857–67.
58. Lee DY, Lee SY, Yun SH, Jeong JW, Kim JH, Kim HW, et al. Review of the current research on fetal bovine serum and the development of cultured meat. *Food Sci Anim Resour.* 2022;42(5):775–99.

Publisher's note

Springer Nature remains neutral with regard to jurisdictional claims in published maps and institutional affiliations.